Chem

CellPress
OPEN ACCESS

Article

Photodynamic treatment of acute vascular occlusion by using an iron–nitrosyl complex

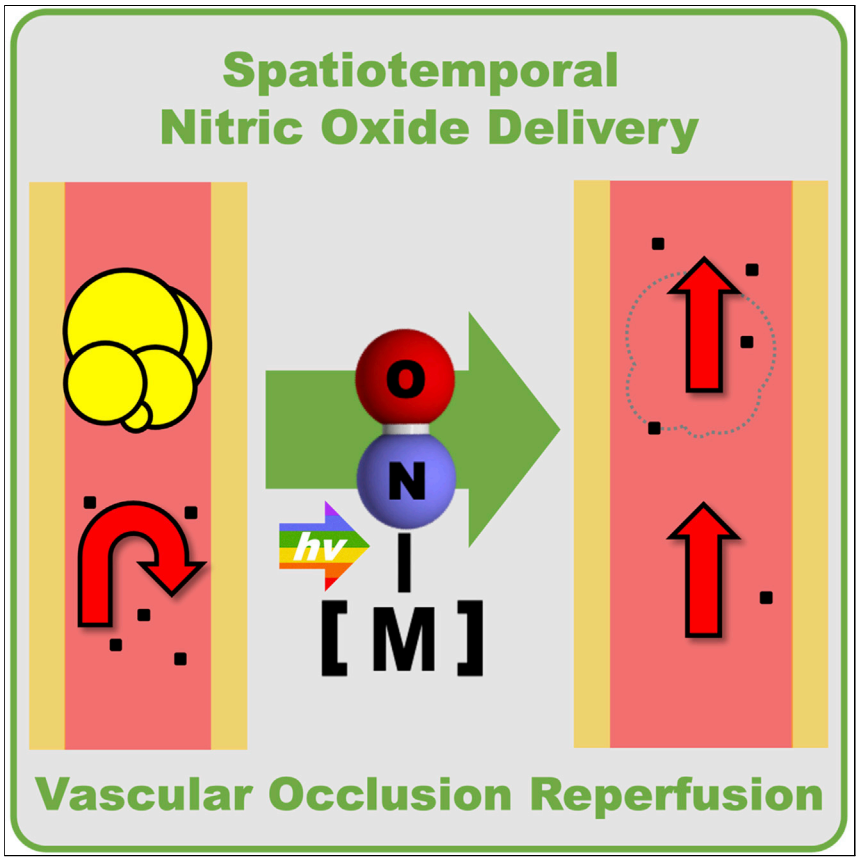

Spatiotemporally controllable nitric oxide transporter, iron–nitrosyl complex, was synthesized and precisely characterized by various physicochemical methods, including X-ray crystallography, together with quantum chemical calculations. Normal retinal blood vessels were expanded by the photoreactive iron–nitrosyl complex. Occluded retinal vessels were effectively reperfused by nitric oxide released from the iron–nitrosyl complex via photoreaction in animal disease models. Our strategy demonstrates potential in the treatment option for acute vascular occlusive diseases.

Jisu Choe, Soo Jin Kim, Jun-Hyeong Kim, Mu-Hyun Baik, Junyeop Lee, Jaeheung Cho

mbaik2805@kaist.ac.kr (M.-H.B.)
j.lee@amc.seoul.kr (J.L.)
jaeheung@unist.ac.kr (J.C.)

Highlights

Development of a spatiotemporally controllable iron–nitrosyl complex

Light-responsive nitric oxide delivery and dilation

Effective reperfusion by photodissociation of an iron–nitrosyl complex

Unprecedented treatment option for acute vascular occlusion

Choe et al., Chem 9, 1309–1317
May 11, 2023
https://doi.org/10.1016/j.chempr.2023.02.013

Chem

CellPress
OPEN ACCESS

Article

Photodynamic treatment of acute vascular occlusion by using an iron–nitrosyl complex

Jisu Choe,[1,2,9] Soo Jin Kim,[3,6,9] Jun-Hyeong Kim,[4,5,9] Mu-Hyun Baik,[4,5,*] Junyeop Lee,[3,6,7,*] and Jaeheung Cho[1,8,10,*]

SUMMARY

Retinal vascular occlusion (RVO) is a common cause of visual impairment. Although several approaches, including vasodilators, have been explored to treat retinal vascular occlusion, there is no proper method to treat this obstruction today. We report a strategy that aims to pierce clogged blood vessels with a spatiotemporally controllable nitric oxide transporter, $[Fe(TBDAP)(NO)(H_2O)]^{2+}$ (1), which was synthesized and precisely characterized by various physicochemical methods, including X-ray crystallography. In the animal model, normal retinal blood vessels were confirmed to be dilated by the photoresponsive iron–nitrosyl complex. Furthermore, occluded retinal blood vessels were effectively reperfused after the immediate delivery of nitric oxide using light in animal disease models. These studies suggest an unprecedentedly selective and controllable treatment option for acute vascular occlusive diseases, including cardiovascular and cerebrovascular diseases.

INTRODUCTION

Nitric oxide (NO), endogenously generated by NO synthase (NOS), is a prominent molecular messenger involved in various physiological processes.[1–4] Specifically, NO plays an essential role as a potent vasodilator, modulating vascular tone, blood pressure, and hemodynamics.[5–8] Due to NO's high diffusion rate and radical character, many NO carriers, including organic compounds and transition metal-based complexes containing NO in their molecular structure, have been investigated.[9,10] Few studies have shown that organic NO donors reduce intraocular pressure in animals, but the level of spatiotemporal control under physiological conditions remains limited.[11] To deal with these limitations, much effort was focused on producing metal–nitrosyl (M–NO) compounds that respond to various stimuli such as pH, solvent, heat, and light to release NO.[9,12–15] Owing to the non-invasiveness and practicability, several photosensitive M–NO adducts have been investigated *in vitro*, leading to the general conclusion that their fast response time is promising for treating acute vascular occlusion diseases.

Retinal vascular occlusion (RVO) that is typically caused by an embolus or thrombus often leads to retinal ischemia, which results in severe and irreversible vision loss,[16] and the number of cases and symptoms emphasizes its seriousness. For example, retinal vein occlusion remains the second most common retinal vascular disease after diabetic retinopathy,[17] and immediate treatments are necessary to relieve retinal arterial occlusion because patients experience acute, profound, and painless visual loss. Systemic vascular diseases such as hypertension, cardiovascular diseases, dyslipidemia, and coagulopathies are risk factors for RVO.[16] Several approaches,

THE BIGGER PICTURE

Obstruction of a blood vessel in our body can cause severe organ damage. Although several conventional vasodilators and thrombolytic agents have previously been considered as treatment, their clinical applications to vascular diseases are limited mainly because of slow reaction time and lack of precise control of their actions. Herein, we report a new therapeutic strategy for piercing clogged blood vessels with a spatiotemporally controllable iron–nitrosyl complex.

Since retinal blood vessels are the only visible and optically accessible blood vessels in the human body, retinal vascular occlusion (RVO) was selected as the first target disease. The photoreactive iron–nitrosyl complex showed not only dilatation of normal retinal blood vessels but also reperfusion of occluded retinal vessels in animal disease models. The strategy provides a scaffold for a new class of therapeutics also relevant for many other cardiovascular and cerebrovascular diseases.

including vasodilators, ocular massage, and anterior chamber paracentesis, have been explored to treat retinal arterial occlusion.[16] But currently, no approved method immediately resolves the causative emboli and reverses retinal damage within the golden time of 3–4 h.[18] Intraocular injection of anti-vascular endothelial growth factor (VEGF) agents is widely used to limit retinal edema secondary to retinal vein occlusion. Nevertheless, VEGF agents have a critical limitation: they do not resolve the causative thrombus and fail to recover the ischemic area completely.[16]

To overcome the limitation of current treatment options for RVO, intraocular delivery of rapidly acting vasodilators is necessary. NO is a promising candidate because it is a potent endothelium-derived vasodilator that plays a significant role in controlling retinal vascular tone and blood flow.[19] Another consideration for the use of vasodilators is to avoid systemic adverse effects. Further, the retina is the only place in the body where light passes directly into the blood vessel. Herein, we present an *in vivo* approach to investigate the NO delivery with temporal and spatial control by a photodissociable iron–nitrosyl complex, $[Fe(TBDAP)(NO)(H_2O)]^{2+}$ (**1**; TBDAP = *N*,*N*′-di-*tert*-butyl-2,11-diaza[3.3](2,6)pyridinophane), which was characterized by X-ray crystallography and a suite of spectroscopic methods as well as quantum chemical calculations. Very recently, we highlighted the artificial control of cell signaling by a cobalt–nitrosyl complex, $[Co(MDAP)(NO)(CH_3CN)]^{2+}$ (**2**; MDAP = *N*,*N*′-dimethyl-2,11-diaza[3.3](2,6)pyridinophane), with light. The chemical properties of **1**, including solubility, are comparable to those of **2**, while the photoresponse behavior differs notably. Kinetic studies demonstrate that the NO release from **1** is slow compared with **2** under similar reaction conditions. Theoretical studies reveal that **1** is much less likely to reach the NO dissociation state than **2**, where the M–NO bond is significantly weakened by metal-to-ligand charge transfer (MLCT) excitation, suggesting that **1** should display slower NO release than **2**. This result affects the reperfusion of RVO significantly and provides further insight into the vasodilation mechanism. We adopted a local NO delivery strategy under temporal and spatial control *in vivo* and validated the possibility of using the M–NO complex to treat RVO.

RESULTS AND DISCUSSION

Synthesis and characterization of 1

The photosensitive iron–nitrosyl complex **1** was prepared by the reaction of excess NO and the iron(II) precursor complex, $[Fe^{II}(TBDAP)(CH_3CN)_2]^{2+}$, in CH_3CN at −40°C under N_2; the color of the solution changed from green to dark red (Figure 1A). Complex **1** was isolated as crystalline solids that were thermally stable at room temperature and soluble in common solvents, such as acetone, CH_3CN, and H_2O. The crystalline sample was used for characterization and *in vivo* studies. The UV-vis spectrum in acetone at −40°C showed characteristic absorption bands of high-spin non-heme $\{FeNO\}^7$ complexes at λ_{max} = 407 (ε = 1,100 M^{-1} cm^{-1}), 522 (ε = 320 M^{-1} cm^{-1}), and 745 nm (ε = 97 M^{-1} cm^{-1}) (Figure 1B).[20–24] The cold-spray ionization mass spectrometry (CSI-MS) spectrum exhibited two prominent ion peaks at a mass-to-charge ratio (*m/z*) of 248.2 and 587.3 (Figure 1C). The mass and isotope distribution patterns corresponded to $[Fe(TBDAP)(NO)(CH_3COCH_3)]^{2+}$ (calcd *m/z* 248.1) and $[Fe(TBDAP)(NO)(OTf)]^{+}$ (calcd *m/z* 587.2), respectively. The Fourier transform infrared (FTIR) spectrum showed a feature at 1,781 cm^{-1} (Figure 1B, inset), which is typical for N–O stretching frequencies of high-spin $\{FeNO\}^7$ complexes containing a Fe^{III}–NO^- moiety (1,720–1,800 cm^{-1}).[20–22,25]

To obtain a direct probe of the ground state, **1** was further characterized by ^1H NMR and electron paramagnetic resonance (EPR) spectroscopy methods. The ^1H NMR

[1]Department of Chemistry, Ulsan National Institute of Science and Technology (UNIST), Ulsan 44919, Republic of Korea

[2]Department of Physics and Chemistry, Daegu Gyeongbuk Institute of Science and Technology (DGIST), Daegu 42988, Republic of Korea

[3]Department of Medical Science, AMIST, Asan Medical Center, University of Ulsan, College of Medicine, Seoul 05505, Republic of Korea

[4]Department of Chemistry, Korea Advanced Institute of Science and Technology (KAIST), Daejeon 34141, Republic of Korea

[5]Center for Catalytic Hydrocarbon Functionalizations, Institute for Basic Science (IBS), Daejeon 34141, Republic of Korea

[6]Department of Ophthalmology, Asan Medical Center, University of Ulsan, College of Medicine, Seoul 05505, Republic of Korea

[7]Translational Biomedical Research Group, Asan Institute for Life Science, Asan Medical Center, Seoul 05505, Republic of Korea

[8]Graduate School of Carbon Neutrality, Ulsan National Institute of Science and Technology (UNIST), Ulsan 44919, Republic of Korea

[9]These authors contributed equally

[10]Lead contact

*Correspondence: mbaik2805@kaist.ac.kr (M.-H.B.), j.lee@amc.seoul.kr (J.L.), jaeheung@unist.ac.kr (J.C.)

https://doi.org/10.1016/j.chempr.2023.02.013

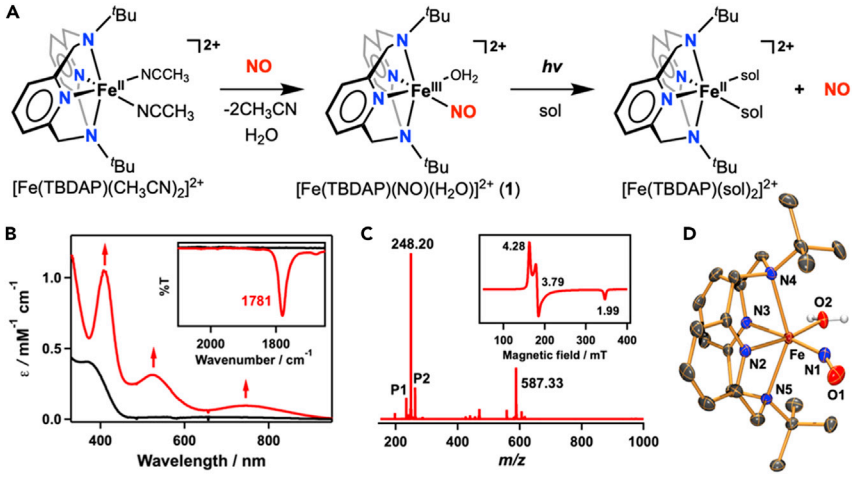

Figure 1. Synthesis and characterization of 1

(A) Schematic illustration of the synthesis and photolysis of **1**.

(B) UV-vis spectra of $[Fe^{II}(TBDAP)(CH_3CN)_2]^{2+}$ (2 mM, black line) and **1** (2 mM, red line) in acetone at −40°C. Inset: FTIR spectra of $[Fe^{II}(TBDAP)(CH_3CN)_2]^{2+}$ (black line) and **1** (red line).

(C) CSI-MS spectrum of **1** in acetone at −40°C. The peak at *m/z* 248.2 for $[Fe(TBDAP)(NO)(CH_3COCH_3)]^{2+}$ and *m/z* 587.3 for $[Fe(TBDAP)(NO)(OTf)]^{+}$. The minor peaks at *m/z* 233.2 (P1) and 262.2 (P2) are assigned to $[Fe(TBDAP)(CH_3COCH_3)]^{2+}$ and $[Fe(TBDAP)(CH_3COCH_3)_2]^{2+}$, respectively. Inset: X-band EPR spectrum of a frozen acetone solution of **1** (7 mM) at 5 K.

(D) Crystal structure of **1** with thermal ellipsoids drawn at 50% probability. Non-essential hydrogen atoms are omitted for clarity. Color for atoms: Fe, scarlet; O, red; N, blue; C, dark gray; H, white. Selected bond lengths (Å) and angle (°): Fe1–N1 1.754(2), Fe1–N2 2.068(2), Fe1–N3 2.063(2), Fe1–N4 2.310(2), Fe1–N5 2.302(2), Fe1–O2 2.0452(19), N1–O1 1.153(3), Fe1–N1–O1 152.9(2).

spectrum in acetone-d_6 showed paramagnetically shifted signals between −20 and 20 ppm, in which the Evans method determined a magnetic moment of 4.31 μ_B. The EPR spectrum in a frozen acetone solution at 5 K exhibited a signal with *g* values of 4.28, 3.79, and 1.99 (Figure 1C, inset). Taken together, all spectroscopic data suggested a Fe^{III}–NO^- ground state (S = 3/2), in which the high-spin Fe^{III} (S = 5/2) and NO^- (S = 1) are antiferromagnetically coupled.[20,23,24,26]

Single crystals suitable for X-ray diffraction were generated by layering diethyl ether into the acetonitrile solution of **1** at −40°C. The X-ray crystal structure for **1**-$(OTf)_2$ reveals a distorted octahedral geometry for the iron center with the N_5O donors composed of a terminal NO, H_2O, and the TBDAP ligand (Figure 1D; Table S1). The N1–O1 and Fe1–N1 bond lengths were 1.153(3) and 1.754(2) Å, respectively, and the Fe1–N1–O1 unit was bent at an angle of 152.9(2)°. These structural parameters are similar to typical six-coordinate high-spin non-heme iron–nitrosyl complexes (N–O = ∼1.14 Å; Fe–N = ∼1.74 Å; Fe–N–O = 146°–165°) (Table S2).[20,23,26–28]

Photoreaction and NO transfer

To confirm the stability of **1** under physiological conditions, spectral changes in the UV-vis absorption band at 407 nm were monitored in H_2O at 37°C (Figure 2A, inset). **1** underwent slow decomposition in an aqueous solution over several minutes. Interestingly, the irradiation of the H_2O solution of **1** with white light (xenon lamp, λ_{irr} = 385–740 nm, 300 W) under N_2 led to a fast decay, as shown in the absorption spectra (Figure 2A, $t_{1/2}$ = 255 s). Under identical conditions, the photolysis of **1** was notably slower than **2** (Figure 2B, $t_{1/2}$ = 24 s). The quantum yield (Φ_{NO}) was found to be 0.23 by employing ferrioxalate as the standard actinometry (see

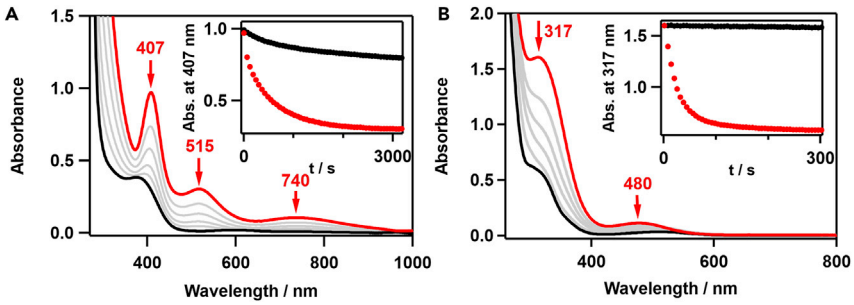

Figure 2. Photodissociation of 1 and 2

Time-resolved UV-vis spectra showing NO dissociation of **1** (1 mM) and **2** (1 mM) in H_2O at 37°C under N_2 upon the photoirradiation under a xenon lamp. Inset: a plot of the absorbance at 407 and 317 nm versus time, showing the decays of **1** and **2** with (red dots) and without (black dots) illumination, respectively.

supplemental information section "experimental section"). The photolysis released NO, and the $[Fe^{II}(TBDAP)(solvent)_2]^{2+}$ product was formed. The NO was captured by [Co(TPP)] (TPP, tetraphenylporphyrinate) to afford [Co(TPP)(NO)], as confirmed by characteristic UV-vis absorption peaks at 414 and 538 nm (Figure S2). The Fe(II) complex produced by photodissociation was detected by electrospray ionization MS (ESI-MS) (Figure S3). In addition, the total amount of NO released was determined to be 0.90 by using the Griess assay (Figure S4).

Computational studies

To better understand the electronic structure and the NO release, complete active space self-consistent field (CASSCF) calculations were carried out (see supplemental information for details). The CAS wavefunction was decomposed into five Fe-d and two NO-π* orbitals, as illustrated in Figure 3A. A total of 5.46 electrons were projected to occupy the MOs dominated by Fe-d orbitals, implying that the iron center is best characterized as being in a Fe^{III}-d^5 configuration. Similarly, 0.91 and 0.80 electrons were found in the NO-π_y* and NO-π_z* orbitals, respectively, suggesting that the NO ligand can be assigned to be anionic. The ground state is dominated by the state function $(d_{x^2-y^2})^{\uparrow}(d_{z^2})^{\uparrow}(d_{yz})^{\uparrow}(d_{xy})^{\uparrow}(d_{xz})^{\uparrow}(\pi_y^*)^{\downarrow}(\pi_z^*)^{\downarrow}$ contributing 47% (Table S4) and representing a state with antiferromagnetic coupling between S = 5/2 Fe^{III} and S = 1 NO^-. Thus, in good agreement with experiments, the computed results are consistent with a Fe^{III}–NO^- assignment for **1**.[29]

Two low-lying excited states of **1** (Q_1 and Q_2) are responsible for the UV-vis band at 740 nm. A detailed analysis of the computer simulation results suggests that a Fe^{I}–NO^+ state, which exists as a minor component in the multiconfigurational ground state, is primarily responsible for the observable excitations. The peak at 740 nm is weak,[29,30] because the Fe^{III}–NO^- configuration is most dominant in the ground state, while the resonance forms $Fe^{I/II/III}$–$NO^{+/\cdot/-}$ that are responsible for the excitation only exist as minor components. The Q_1 and Q_2 states primarily consist of a Fe^{II}–$NO^{\cdot}$ state function, most easily reached by MLCT from the Fe^{I}–NO^+ configurations (Table S6). Specifically, these transitions promote electron transfer from an Fe-d-dominated Fe–NO bonding orbital to a NO-π*-dominated Fe–NO antibonding orbital. Thus, these MLCT excitations at 740 nm will weaken the Fe–NO bond and promote NO release (Figure S7). We envision that the NO moiety will undergo ligand exchange with a solvent molecule or be released by the Fe–NO stretching motion in a unimolecular fashion.[31] The MLCT assignment explains why **1** may show higher persistence upon irradiation[14] than **2**. Similar to **1**, our calculations

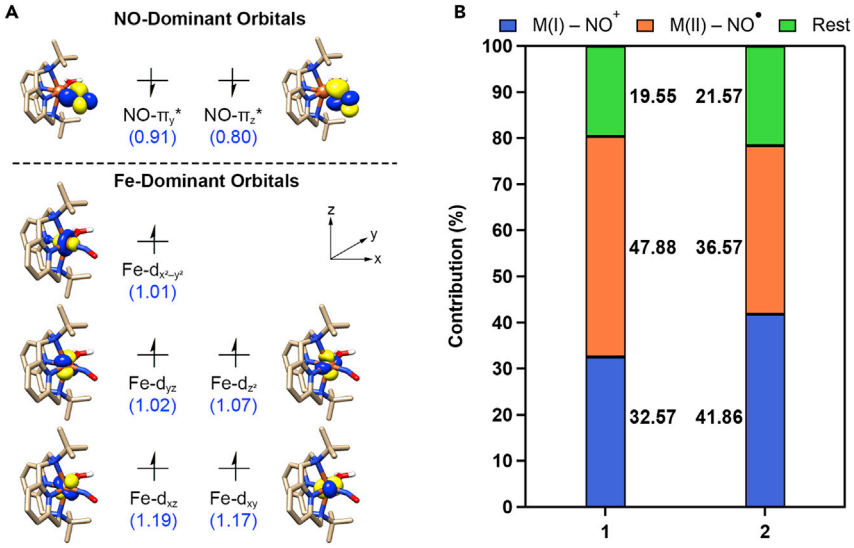

Figure 3. Computational studies on 1 and 2

(A) Ground-state electronic structure of **1** computed at the CASSCF(11,9)/def2-TZVP level of theory with a single root. The CAS wavefunction is projected into the Foster-Boys localized orbital manifold for visualization. Non-essential hydrogen atoms are omitted for clarity, and an isodensity value of 0.05 e/Å^3 is used for the orbital plots. Average occupation numbers are given in blue.

(B) The bar graphs highlight the M–NO$^+$ configuration percentage of **1** and **2** involved in reaching the MLCT state.

assign MLCT transition to the band at 480 nm, which promotes the photolysis of **2** (Table S8). Most importantly, **2** is more likely to reach the MLCT state than **1** (42% versus 33%), as conceptualized in Figure 3B. These percentages reflect the probability of MLCT and indicate that **2** should show a greater quantum yield and shorter lifetime due to NO photodissociation.

Therapeutic efficacy of 1 and 2 for RVO

Taking advantage of the fact that the retinal vasculature can be examined without invasive procedures, we evaluated the mouse retina's vasodilatory function of both M–NO species. First, the M–NO species were administered into the eye by intravitreal injection. Then, strong pin lights were directed to the eyes for the optimal duration to induce the NO release, using a medical pen light (clip light 5 mm LED, λ_{irr} = 450–700 nm). As anticipated, both **1** and **2** caused significant vasodilation, but **1** was notably more potent, showing a 1.59-fold increase in vessel diameter within 15 min of light exposure. By contrast, a more moderate increase of 1.32-fold within 5 min was seen for **2** (Figure S12). Without light, neither **1** nor **2** exhibited vessel dilation (Figure S13).

The mouse RVO was modeled by intravenously injecting Rose Bengal and inducing photocoagulation by a focal green laser.[32,33] The potential value of the M–NO compounds for photodynamic therapy was evaluated by determining whether reperfusion can be induced after the occlusion of retinal blood vessels in the animal model (Figure 4A). The generation of the RVO model was confirmed by intravital imaging of the retinal blood vessels (Figure 4B).

The RVO mice treated with **2** did not show any significant FITC-dextran perfusion over the occlusion site, similarly to what was seen for the distilled water(D.W.)-treated control (Figure 4B; empty arrowhead). By contrast, mice treated with **1** displayed

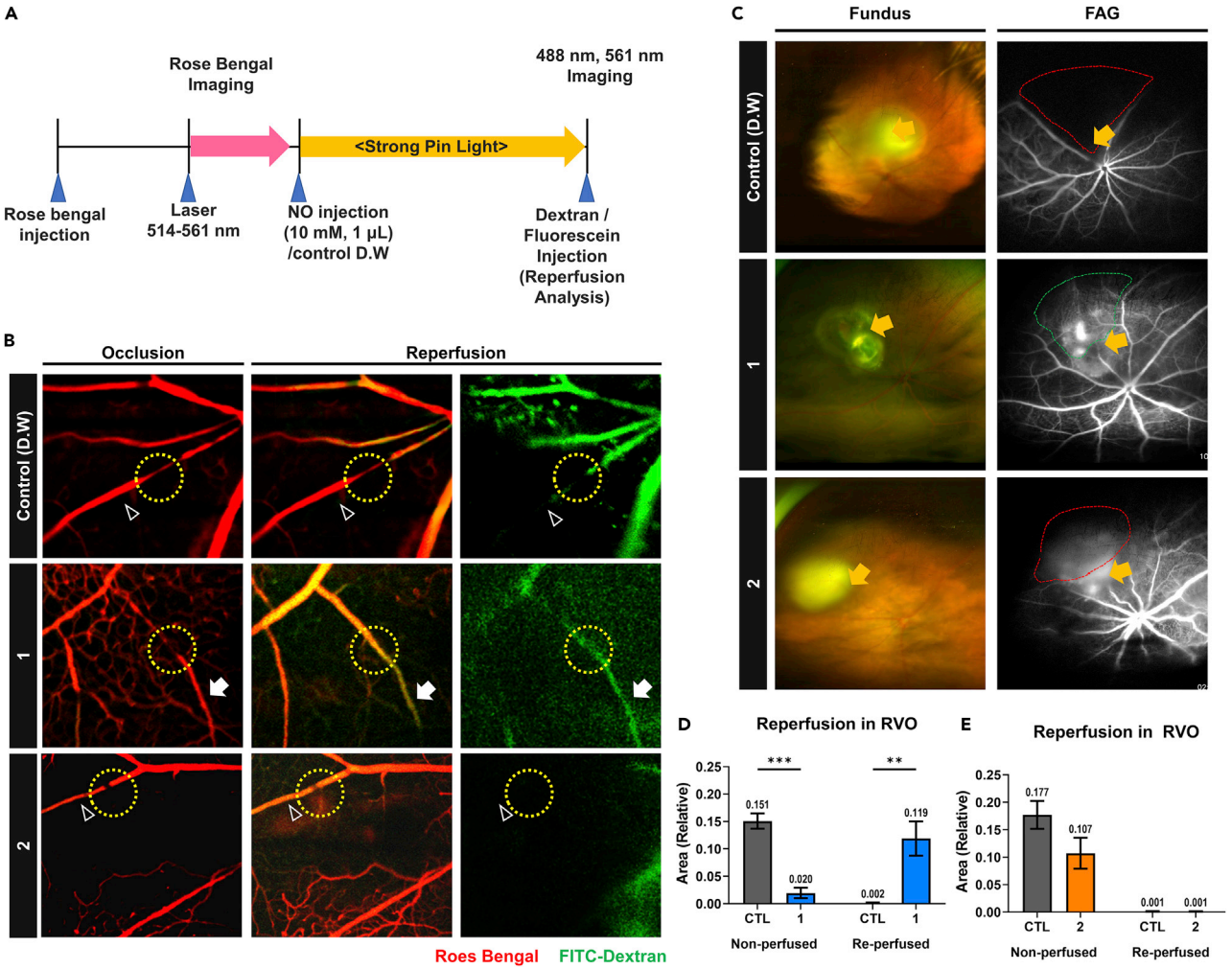

Figure 4. 1 induces the reperfusion of the ischemic retinal area in the RVO model

(A) Diagram for retinal vascular occlusion (RVO) model generation.

(B) Intravital images of the RVO generation and reperfusion. Live fluorescent microscopy of the occlusion spot (dashed yellow circle), non-perfused vessels (white blank arrowhead), and reperfused vessels (solid white arrow).

(C) Ultra-widefield fundus photography at occlusion (solid yellow arrow).

(D and E) FA for branched peripheral microvessels, non-perfused (dashed red line), and reperfused (dashed green line) are indicated and analyzed in (D) and (E). Error bars: SD, **$p < 0.01$ and ***$p < 0.001$ versus control by Student's t test ($n = 4$).

perfusion beyond the vascular occlusion sites (Figure 4B; solid arrow), suggesting the successful opening of occluded blood vessels. The RVO rescue efficacy of **1** was also evident in the intravital ultra-widefield (UWF) fundus photo and fluorescence angiography (FA). Eyes treated with **1** showed more than 85% recovery of the non-perfused peripheral retinal area at the FA from the occlusion site. In addition, only a small area nearby the laser photocoagulation sites remained ischemic (Figures 4C and 4D). On the other hand, **2** did not rescue the non-perfusion area in this RVO model (Figures 4C and 4E). Therefore, we hypothesize that the superior therapeutic efficacy of **1** is derived from the slower photoresponse behavior. The slower response afforded a longer-lasting and sustained release of NO capable of vasodilation and reperfusion.

We next evaluated how fast **1** can restore blood perfusion by focusing on the occluded site. The occluded vessel was reperfused up to about 46% of its original

perfusion diameter 10 min after injection (Figures S14A and S14B). The dose-dependent efficacy of **1** was also evaluated *in vivo*, using three different doses, 1, 5, and 10 mM. For the full recovery of the non-perfused area, the 5 and 10 mM doses required ~15 min, but the 1 mM dose showed an effect 30 min after injection (Figures S14C and S14D). As positive controls, the NO-releasing donors diethylenetriamine diazeniumdiolates (DETA-NONOate)[34] and sodium nitroprusside (SNP)[9] were evaluated under identical conditions. DETA-NONOate and SNP restored the perfusion in the RVO models (Figures S15A and S15B); however, exudative retinal detachment occurred 10 min after injection and progressed over time (Figures S15C and S15D). This adverse event is attributed to the breakdown of the blood-retinal barrier due to excessive vasodilation and fluid leakage.

By contrast, this vision-threatening adverse effect was not observed in the test groups treated with M–NO in combination with light exposure. M–NO with high stability and selective photoreactivity can regulate the amount of NO release, highlighting that it is essential for the NO-mediated therapy to precisely control the amount and duration of NO release to prevent serious adverse effects. NO activates soluble guanylyl cyclase to form cyclic guanosine monophosphate (cGMP), and increased cGMP levels in vascular cells are associated with NO-induced vasodilation.[35] In the tissue lysate from the eyes treated with the **1** and DETA-NONOate, the cGMP concentration was significantly increased, compared with the control (Figure S16).

Here, we demonstrated that intravitreal injection of the M–NO compounds **1** and **2** combined with transient light exposure dramatically dilated retinal blood vessels, opened the closure sites rapidly, and induced reperfusion in the RVO animal models. This rapid blood flow recovery within several minutes prevents ischemic neuronal damage and maintains visual acuity. Based on these findings, we propose this novel method as a promising therapeutic option for treating RVO disorders. Intravitreal injection is a simple procedure usually performed in an outpatient clinic under topical anesthesia. The localized treatment with the M–NO compounds can avoid the potential risks of intracranial hemorrhage, remote embolism, hypertensive crisis, hematuria, and stroke, which could occur as side effects after intravenous or intra-arterial thrombolysis. Moreover, the visual outcomes post thrombolysis were heterogeneous.[36] Because the compound injection with light exposure easily adjusts the dose of molecules and intensity of light, this strategy may be effective for treating other retinal vascular diseases, including diabetic retinopathy and age-related macular degeneration.

Conclusions

Reperfusion of retinal large vessel occlusion by a photosensitive iron–nitrosyl complex, $[Fe(TBDAP)(NO)(H_2O)]^{2+}$ (**1**), has been achieved in the present work. The isolable compound **1** was prepared by reacting an iron(II) precursor and gaseous NO. The Fe^{III}–NO^- core was characterized by spectroscopic and structural methods, including X-ray crystallographic analysis. The photolysis of NO from **1** was confirmed by NO capturing experiments with [Co(TPP)] and the Griess assay. The photodissociation of **1** ($t_{1/2}$ = 255 s) is much slower than that of the cobalt–nitrosyl complex, **2** ($t_{1/2}$ = 24 s). Quantum chemical calculations support the Fe^{III}–NO^- assignment, where a triplet NO moiety is antiferromagnetically coupled to a high-spin Fe(III) center. The photolysis mechanism involves MLCT transitions by near-IR light, which initiates NO release. Both compounds were effective at retinal blood vessel dilation, but only complex **1** showed vascular reperfusion due to sustained NO delivery over a more extended period. Our approaches and findings on reperfusion of the retinal vessel occlusion, along with the detailed molecular-level understanding,

demonstrate the feasibility of utilizing the metal–nitrosyl complexes for the photodynamic treatment of vascular occlusion.

EXPERIMENTAL PROCEDURES

Resource availability

Lead contact

Further information and requests for resources should be directed to and will be fulfilled by the lead contact, Jaeheung Cho (jaeheung@unist.ac.kr).

Materials availability

All materials generated in this study are available from the lead contact.

Data and code availability

All data generated or analyzed during this study are available within this article (and its supplemental information including Tables S10 and S11). Crystallographic data are available free of charge from the Cambridge Crystallographic Data Centre (CCDC): 2127235.

SUPPLEMENTAL INFORMATION

Supplemental information can be found online at https://doi.org/10.1016/j.chempr.2023.02.013.

ACKNOWLEDGMENTS

The research was supported by the National Research Foundation funded by the Ministry of Science, ICT and Future Planning of Korea (2019R1A2C2086249 to J. Cho), National Research Foundation of Korea (NRF) grant funded by the Korean government (the Ministry of Science and ICT, MSIT) (2018R1A5A1025511 to J.L.), and the Institute for Basic Science in Korea (IBS-R010-A1 to M.-H.B.).

AUTHOR CONTRIBUTIONS

J. Cho, J.L., and M.-H.B. conceived and designed the experiments. J. Choe and S.J.K. performed the experiments. J.-H.K. conducted quantum chemical calculations. All authors analyzed the data, discussed the results, and co-wrote the manuscript.

DECLARATION OF INTERESTS

The authors declare no competing interests.

INCLUSION AND DIVERSITY

We support inclusive, diverse, and equitable conduct of research.

Received: September 20, 2022
Revised: December 29, 2022
Accepted: February 16, 2023
Published: March 15, 2023

REFERENCES

1. Ignarro, L.J. (2000). Nitric Oxide: Biology and Pathobiology (Academic Press).

2. Culotta, E., and Koshland, D.E. (1992). NO news is good news. Science *258*, 1862–1865. https://doi.org/10.1126/science.1361684.

3. Tennyson, A.G., and Lippard, S.J. (2011). Generation, translocation, and action of nitric oxide in living systems. Chem. Biol. *18*, 1211–1220. https://doi.org/10.1016/j.chembiol.2011.09.009.

4. Toledo, J.C., and Augusto, O. (2012). Connecting the chemical and biological properties of nitric oxide. Chem. Res. Toxicol. *25*, 975–989. https://doi.org/10.1021/tx300042g.

5. Levine, A.B., Punihaole, D., and Levine, T.B. (2012). Characterization of the role of nitric oxide and its clinical applications. Cardiology *122*, 55–68. https://doi.org/10.1159/000338150.

6. Martínez-Ruiz, A., and Lamas, S. (2004). Detection and proteomic identification of S-nitrosylated proteins in endothelial cells. Arch. Biochem. Biophys. *423*, 192–199. https://doi.org/10.1016/j.abb.2003.12.006.

7. Maron, B.A., Tang, S.-S., and Loscalzo, J. (2013). *S*-nitrosothiols and the *S*-nitrosoproteome of the cardiovascular system. Antioxid. Redox Signal. *18*, 270–287. https://doi.org/10.1089/ars.2012.4744.

8. Farah, C., Michel, L.Y.M., and Balligand, J.-L. (2018). Nitric oxide signalling in cardiovascular health and disease. Nat. Rev. Cardiol. *15*, 292–316. https://doi.org/10.1038/nrcardio.2017.224.

9. Wang, P.G., Xian, M., Tang, X., Wu, X., Wen, Z., Cai, T., and Janczuk, A.J. (2002). Nitric oxide donors: Chemical activities and biological applications. Chem. Rev. *102*, 1091–1134. https://doi.org/10.1021/cr000040l.

10. Li, L., and Li, L. (2016). Recent advances in multinuclear metal nitrosyl complexes. Coord. Chem. Rev. *306*, 678–700. https://doi.org/10.1016/j.ccr.2015.03.026.

11. Serafim, R.A.M., Primi, M.C., Trossini, G.H.G., and Ferreira, E.I. (2012). Nitric oxide: State of the art in drug design. Curr. Med. Chem. *19*, 386–405. https://doi.org/10.2174/092986712803414321.

12. Ke, C.-H., Chen, C.-H., Tsai, M.-L., Wang, H.-C., Tsai, F.-T., Chiang, Y.-W., Shih, W.-C., Bohle, D.S., and Liaw, W.-F. (2017). $\{Fe(NO)_2\}^9$ dinitrosyl iron complex acting as a vehicle for the NO radical. J. Am. Chem. Soc. *139*, 67–70. https://doi.org/10.1021/jacs.6b11454.

13. Dey, A., Confer, A.M., Vilbert, A.C., Moënne-Loccoz, P., Lancaster, K.M., and Goldberg, D.P. (2018). A nonheme sulfur-ligated $\{FeNO\}^6$ complex and comparison with redox-interconvertible $\{FeNO\}^7$ and $\{FeNO\}^8$ analogues. Angew. Chem. Int. Ed. *57*, 13465–13469. https://doi.org/10.1002/anie.201806146.

14. Shin, S., Choe, J., Park, Y., Jeong, D., Song, H., You, Y., Seo, D., and Cho, J. (2019). Artificial control of cell signaling using a photocleavable cobalt(III)–nitrosyl complex. Angew. Chem. Int. Ed. *58*, 10126–10131. https://doi.org/10.1002/anie.201903106.

15. Hsieh, C.-H., and Darensbourg, M.Y. (2010). A $\{Fe(NO)_3\}^{10}$ trinitrosyliron complex stabilized by an N-heterocyclic carbene and the cationic and neutral $\{Fe(NO)_2\}^{9/10}$ products of its NO release. J. Am. Chem. Soc. *132*, 14118–14125. https://doi.org/10.1021/ja104135x.

16. Scott, I.U., Campochiaro, P.A., Newman, N.J., and Biousse, V. (2020). Retinal vascular occlusions. Lancet *396*, 1927–1940. https://doi.org/10.1016/S0140-6736(20)31559-2.

17. Jaulim, A., Ahmed, B., Khanam, T., and Chatziralli, I.P. (2013). Branch retinal vein occlusion: epidemiology, pathogenesis, risk factors, clinical features, diagnosis, and complications. An update of the literature. Retina *33*, 901–910. https://doi.org/10.1097/IAE.0b013e3182870c15.

18. Hayreh, S.S., Kolder, H.E., and Weingeist, T.A. (1980). Central retinal artery occlusion and retinal tolerance time. Ophthalmology *87*, 75–78. https://doi.org/10.1016/S0161-6420(80)35283-4.

19. Dorner, G.T., Garhofer, G., Kiss, B., Polska, E., Polak, K., Riva, C.E., and Schmetterer, L. (2003). Nitric oxide regulates retinal vascular tone in humans. Am. J. Physiol. Heart Circ. Physiol. *285*, H631–H636. https://doi.org/10.1152/ajpheart.00111.2003.

20. Berto, T.C., Speelman, A.L., Zheng, S., and Lehnert, N. (2013). Mono- and dinuclear non-heme iron–nitrosyl complexes: models for key intermediates in bacterial nitric oxide reductases. Coord. Chem. Rev. *257*, 244–259. https://doi.org/10.1016/j.ccr.2012.05.007.

21. Jana, M., Pal, N., White, C.J., Kupper, C., Meyer, F., Lehnert, N., and Majumdar, A. (2017). Functional mononitrosyl diiron(II) complex mediates the reduction of NO to N_2O with relevance for flavodiiron NO reductases. J. Am. Chem. Soc. *139*, 14380–14383. https://doi.org/10.1021/jacs.7b08855.

22. Jana, M., White, C.J., Pal, N., Demeshko, S., Cordes, C., Meyer, F., Lehnert, N., and Majumdar, A. (2020). Functional models for the mono- and dinitrosyl intermediates of FNORs: semireduction versus superreduction of NO. J. Am. Chem. Soc. *142*, 6600–6616. https://doi.org/10.1021/jacs.9b13795.

23. Li, J., Banerjee, A., Pawlak, P.L., Brennessel, W.W., and Chavez, F.A. (2014). Highest recorded N–O stretching frequency for 6-coordinate $\{Fe\text{-}NO\}^7$ complexes: an iron nitrosyl model for His_3 active sites. Inorg. Chem. *53*, 5414–5416. https://doi.org/10.1021/ic500558j.

24. Confer, A.M., Sabuncu, S., Siegler, M.A., Moënne-Loccoz, P., and Goldberg, D.P. (2019). Mononuclear, nonheme, high-spin $\{FeNO\}^{7/8}$ complexes supported by a sterically encumbered N_4S-thioether ligand. Inorg. Chem. *58*, 9576–9580. https://doi.org/10.1021/acs.inorgchem.9b01475.

25. Zhang, Y., Pavlosky, M.A., Brown, C.A., Westre, T.E., Hedman, B., Hodgson, K.O., and Solomon, E.I. (1992). Spectroscopic and theoretical description of the electronic structure of the $S = 3/2$ nitrosyl complex of non-heme iron enzymes. J. Am. Chem. Soc. *114*, 9189–9191. https://doi.org/10.1021/ja00049a062.

26. Brown, C.A., Pavlosky, M.A., Westre, T.E., Zhang, Y., Hedman, B., Hodgson, K.O., and Solomon, E.I. (1995). Spectroscopic and theoretical description of the electronic structure of $S = 3/2$ iron–nitrosyl complexes and their relation to O_2 activation by non-heme iron enzyme active sites. J. Am. Chem. Soc. *117*, 715–732. https://doi.org/10.1021/ja00107a015.

27. Berto, T.C., Hoffman, M.B., Murata, Y., Landenberger, K.B., Alp, E.E., Zhao, J., and Lehnert, N. (2011). Structural and electronic characterization of non-heme Fe(II)-nitrosyls as biomimetic models of the Fe_B center of bacterial nitric oxide reductase. J. Am. Chem. Soc. *133*, 16714–16717. https://doi.org/10.1021/ja111693f.

28. Chiou, Y.-M., and Que, L., Jr. (1995). Model studies of α-keto acid-dependent nonheme iron enzymes: nitric oxide adducts of $[Fe^{II}(L)(O_2CCOPh)](ClO_4)$ complexes. Inorg. Chem. *34*, 3270–3278. https://doi.org/10.1021/ic00116a020.

29. Radoń, M., Broclawik, E., and Pierloot, K. (2010). Electronic structure of selected $\{FeNO\}^7$ complexes in heme and non-heme architectures: A density functional and multireference ab initio study. J. Phys. Chem. B *114*, 1518–1528. https://doi.org/10.1021/jp910220r.

30. Van Leest, N.P., Tepaske, M.A., Oudsen, J.-P.H., Venderbosch, B., Rietdijk, N.R., Siegler, M.A., Tromp, M., Van Der Vlugt, J.I., and De Bruin, B. (2020). Ligand redox noninnocence in $[Co^{III}(TAML)]^{0/-}$ complexes affects nitrene formation. J. Am. Chem. Soc. *142*, 552–563. https://doi.org/10.1021/jacs.9b11715.

31. Vorobyev, V., Budkina, D.S., and Tarnovsky, A.N. (2020). Femtosecond excited-state dynamics and nitric oxide photorelease in a prototypical ruthenium nitrosyl complex. J. Phys. Chem. Lett. *11*, 4639–4643. https://doi.org/10.1021/acs.jpclett.0c01105.

32. Ebneter, A., Agca, C., Dysli, C., and Zinkernagel, M.S. (2015). Investigation of retinal morphology alterations using spectral domain optical coherence tomography in a mouse model of retinal branch and central retinal vein occlusion. PLoS One *10*, e0119046. https://doi.org/10.1371/journal.pone.0119046.

33. Khayat, M., Lois, N., Williams, M., and Stitt, A.W. (2017). Animal models of retinal vein occlusion. Invest. Ophthalmol. Vis. Sci. *58*, 6175–6192. https://doi.org/10.1167/iovs.17-22788.

34. Li, B., Ming, Y., Liu, Y., Xing, H., Fu, R., Li, Z., Ni, R., Li, L., Duan, D., Xu, J., et al. (2020). Recent developments in pharmacological effect, mechanism and application prospect of diazeniumdiolates. Front. Pharmacol. *11*, 923. https://doi.org/10.3389/fphar.2020.00923.

35. Archer, S.L., Huang, J.M., Hampl, V., Nelson, D.P., Shultz, P.J., and Weir, E.K. (1994). Nitric oxide and cGMP cause vasorelaxation by activation of a charybdotoxin-sensitive K channel by cGMP-dependent protein kinase. Proc. Natl. Acad. Sci. USA *91*, 7583–7587. https://doi.org/10.1073/pnas.91.16.7583.

36. Dumitrascu, O.M., Newman, N.J., and Biousse, V. (2020). Thrombolysis for central retinal artery occlusion in 2020: time is vision! J. Neuroophthalmol. *40*, 333–345. https://doi.org/10.1097/WNO.0000000000001027.